Radial granular segregation under chaotic flow in two-dimensional tumblers

Stephen E. Cisar,[1] Paul B. Umbanhowar,[2,*] and Julio M. Ottino[1]
[1]*Department of Chemical and Biological Engineering, Northwestern University, Evanston, Illinois 60208, USA*
[2]*Department of Physics and Astronomy, Northwestern University, Evanston, Illinois 60208, USA*
(Received 24 February 2006; revised manuscript received 5 July 2006; published 15 November 2006)

An initially well mixed granular material composed of two distinct subclasses of particles, small and large or light and heavy, segregates radially into stable lobed patterns when rotated in various quasi-two-dimensional, regular polygonal tumblers. The patterns are highly sensitive to the time-periodic flow, which in turn depends critically on the fill fraction and container shape. Simulations of a simple model reproduce the segregation patterns observed in experiment. Kolmogorov-Arnol'd-Moser (KAM) regions in Poincaré plots of the velocity field used to model the flow attract smaller (denser) particles and their spatial symmetries mirror those of the segregation patterns, suggesting that competition between the driving forces for radial segregation (percolation and buoyancy) and those for chaotic mixing plays a key role.

DOI: 10.1103/PhysRevE.74.051305 PACS number(s): 45.70.Mg, 45.70.Qj, 47.52.+j, 47.57.Gc

I. INTRODUCTION

An intriguing property of granular matter is the tendency of particles with slightly different properties, such as size or density, to segregate. In nature, segregation is evident in the structure of sedimentary rocks, the distribution of material in rivers, rock fields, and avalanches. Segregation also has important implications in industrial processes where it works against the goal of mixing. In recent years the flow of and patterns produced by granular materials have received an increasing amount of attention [1]. The interest is due not only to the wide variety of granular flows that can be found in nature and technology but also to the range of intriguing behaviors exhibited by driven granular matter in the lab.

A common way to mix particles in industry is through the use of partially filled rotating tumblers, with the simplest case being an axially rotated horizontal cylindrical drum. Henein *et al.* [2] showed that in this geometry particle flow can be categorized into four regimes—avalanching, continuous, cataracting, and centrifuging [3]—depending on the Froude number of the system (the ratio of rotational to gravitational forces) and the particle size. For very low rotation rates, relative particle motion occurs in discrete avalanches. As the rotation rate is increased the interval between avalanches becomes shorter until a continuous flow of particles is realized. Rajchenbach [4] observed hysteresis in this transition. As the rotation rate is increased further, the initially flat surface becomes S shaped, which is the primary characteristic of the cataracting regime. Finally, for fast rotation, particles move to and become pinned at the edges of the tumbler (centrifuging); the material ultimately moves in pure solid body rotation with no relative motion of particles. Tumblers with small length to diameter ratios have negligible axial particle flow and are referred to as quasi-two-dimensional (2D). A simple continuum model for the continuous flow regime in quasi-2D tumblers was developed by Khakhar *et al.* [5,6] for monodisperse systems. When mixtures of particles of different sizes (*S* systems) or different densities (*D* systems) are placed in a short cylindrical tumbler a core of smaller (or denser) particles forms quickly upon rotation; this radial segregation occurs in $O(1)$ revolution. Hill *et al.* [7,8] studied mixing and segregation in noncircular tumblers and found chaotic flow and segregation patterns with additional structure. While these patterns vary slightly throughout a single tumbler revolution, the same structure is observed at the end of every revolution [8]. In this sense, the patterns are said to be stable and time-independent. The exact nature of the segregation and mixing trends is sensitive to fill fraction (the percentage of the tumbler volume occupied by the granular material) and other parameters making prediction difficult in all but the simplest cases.

Near the free surface, particles in the "flowing layer" continually roll, slide, and collide as they move downslope. Below the flowing layer in the "fixed bed," relative particle motion is much reduced and friction dominates the dynamics [9]. This slow creeping/plastic flow region is similar to that observed in flow down heaps by Komatsu *et al.* [10], and is only evident after thousands of rotations. On the other hand, mixing and segregation of the tumbler contents occur in $O(10)$ rotations. Therefore, for modeling segregation processes, the tumbler is effectively divided into two distinct regions: One in which particles undergo pure solid body rotation, and another lens-shaped one in which particles move downhill in a simple shear flow.

In this paper, we use experiment (*S* systems) and simulation (*D* systems) to study the segregation of binary mixtures in a variety of regular polygonal tumblers. Poincaré sections constructed from the motion of passive scalars, advected by a continuum model of the flow field, show that the structure of segregation patterns is closely linked to the existence of islands of regular flow that surround elliptic points. The locations of these points, which are quite sensitive to the tumbler fill level, are predicted by a simple geometric picture.

II. EXPERIMENT

The experimental apparatus consists of a tumbler partially filled with different-sized glass beads, rotated horizontally about its axis with constant angular velocity. The tumbler is

*Electronic address: umbanhowar@northwestern.edu

made from a stack of four squares of acrylic with side length 25 cm and thicknesses 3.0, 6.35, 3.0, and 15.0 mm. The 6.35 mm thick piece has a central square cavity with a side length of 15.8 cm. Square posterboard inserts with single, centered, regular polygonal-shaped voids—having three to eight sides—are placed within the cavity. The distance from the void center to each void corner is 6.8 cm. A sheet of white laminated paper between the third and fourth acrylic sheets (3 mm and 15 mm) provides a uniform background for imaging. The acrylic sheets are fastened together and attached to a computer-controlled Compumotor LE357-51 stepper motor. Images of the tumbler are taken with a Kodak DC4800 digital camera.

The granular mixture consists of glass beads with diameters, d, of 0.3 ± 0.05 mm (painted black) and 0.85 ± 0.06 mm (clear). Mixtures are prepared by combining by volume one part small (black) particles and two parts by large (clear) particles. In the experiments, the volumetric fill fraction ϕ is varied from 0.50–0.85 in increments of 0.05 for all six tumbler shapes. Mixtures are placed in the insert void, and a well-mixed initial condition is prepared by stirring the granular mixture *in situ* before closing the tumbler. The tumbler is rotated clockwise at 2 revolutions per minute (RPM) until the segregation patterns are steady, which usually occurs within five revolutions.

In experiments the ratio of the tumbler length l to particle diameter is important. If this ratio is too small, particle crystallization and jamming result, while if it is too large, significant axial movement occurs. These effects are insignificant in our experiments since the tumbler length to average particle diameter ratio is around 20.

III. FLOW MODELING

To study the motion and associated segregation of granular material within rotating tumblers, we use a two-dimensional model which combines a continuum description with discrete particle dynamics. The underlying flow is described by a continuum model and is characterized by Poincaré sections constructed from the motion of passive scalars advected by the flow. To study segregation, we introduce a bidisperse population of active particles that, in addition to being advected by the continuum flow, interact with each other via an effective buoyancy term and undergo collisional diffusion.

A. Continuum flow

Our model of the tumbler velocity field is based on the single phase, incompressible, continuum flow description of Khakhar *et al.* [5,6] in which a cylinder with radius R and length l (where $R \gg l$ so that the system is effectively two dimensional) rotates at constant angular velocity ω in the continuous flow regime. In this regime, particles well below the free surface move in solid body rotation with the tumbler in a region called the fixed bed, while near the free surface particles move relative to each other in a lens shaped shear region designated as the flowing layer. Particles initially in the fixed bed are transported toward the free surface and into the flowing layer. Then, with respect to a diameter through the middle of the flowing layer, particles move downhill to a position roughly opposite to where they entered the flowing layer. Here they rejoin the fixed bed and the process repeats.

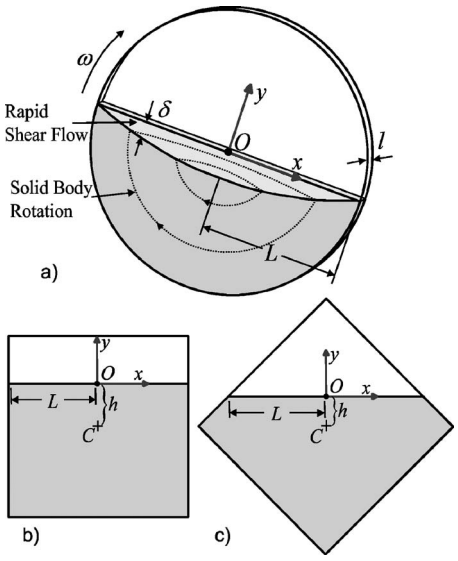

FIG. 1. (a) Diagram of the circular tumbler with the coordinate system and parameters defined. (b), (c) Two configurations of a 75% full square tumbler with vertically translating coordinate systems. Note that the length of the free surface increases from (b) to (c) while the height of the free surface decreases.

Figure 1 illustrates the geometry, parameters, and coordinates used to describe our system. A right-hand coordinate system is defined with origin O at the center of the free surface. The x axis points downhill along the free surface while the positive y axis is normal to and points away from the free surface. [Note that in all figures of the tumbler system with the exception of Fig. 1(a) the perspective is rotated by the dynamic angle of repose (approximately 30°) so that the free surface is horizontal.] The depth of the flowing layer δ [see Fig. 1(a)] is given by

$$\delta = \delta_0 \left[1 - \left(\frac{x}{L} \right)^2 \right], \tag{1}$$

where δ_0 is the maximum depth and L is the layer half length [6]. Assuming a linear shear profile, the tangential velocity is

$$v_x = 2u \left(1 + \frac{y}{\delta} \right), \tag{2}$$

where u is the depth averaged velocity of the flowing layer. If one further assumes that u is constant along the layer and the flow is incompressible, the continuity equation can be used to determine the normal velocity

$$v_y = -\omega x \left(\frac{y}{\delta} \right)^2. \tag{3}$$

Setting the mass flux into the flowing layer or, equivalently, through $\delta(x)$, for $-L<x<0$ equal to the mass flux through the middle of the flowing layer (i.e., $x=0$, $-\delta_0<y<0$) we obtain a depth averaged velocity $u=\omega L^2/2\delta_0$. The shear rate

$\dot{\gamma}$ then varies with x and is equal to $2u/\delta(x)$. Particles not in the flowing layer are assumed to undergo solid body rotation with angular velocity ω. Since the speed of particles within the flowing layer is typically large compared to $\omega\sqrt{x^2+y^2}$, velocity contributions due to solid body rotation are ignored within the flowing layer.

Arguments have been made for the use of the layer profile $\tilde{\delta}=\delta_0[1-(x/L)^2]^{1/2}$ (Makse [11], Khakhar *et al.* [12]). In this case the resulting mass balance gives $v_x \sim yx$ and $v_y \sim y/x$ as opposed to $v_x \sim y/x^2$ and $v_y \sim y^2/x^4$ for the profile used above in Eq. (1). Our simulations show that both profiles produce similar mixing and Poincaré sections. However, simulations using $\tilde{\delta}$ are more sensitive to numerical errors, so generally the profile in Eq. (1) is preferable. Elperin and Vikhansky employed a layer depth that scales with $x^{4/5}$ [13]. However, their model applies at the transition to cataracting flow where the free surface is no longer flat.

For circular tumblers the mean velocity field is time independent. However, if the angular velocity is varied [14] and/or the tumbler is not rotationally invariant, the flow becomes time dependent and the model must be modified. In particular, the length, depth, position, and mean velocity u of the flowing layer vary as the tumbler rotates [see Figs. 1(b) and 1(c)]. For a given tumbler orientation the fill fraction determines the position, shape, and size of the free surface, and consequently the location of the coordinate origin. To determine the variation in u we rely on recent experimental measurements in various 3D geometries that indicate the surface velocity and therefore u scales with L (Pohlman *et al.* [15]). Note that if $u \sim L$ then $\delta_0 \sim L$ (since $u=\omega L^2/2\delta_0$). In experiments δ_0 is typically 5–15 particle diameters and linearly dependent on L [9]. Here we use $\delta_0=L/10$. This completes the underlying fluid mechanical or continuum description of the flow.

For any quasi-2D tumbler rotated at a constant rate the stream function is time-periodic, i.e., $\psi(x,y,t)=\psi(x,y,t+T/N)$, where $T=2\pi/\omega$ is the rotation period and $T' \equiv T/N$ is the period of the stream function (flow period). In general, N is the number of flow periods per tumbler revolution, while in the specific case of a regular polygonal tumbler it is equal to the number of sides. The Poincaré sections associated with the stream function are generated by plotting the location of passive scalar particles advected by the flow given by Eqs. (2) and (3) every T'. In our simulations 13 noninteracting particles equally spaced along a line from the center of the tumbler to a corner are advected with velocities determined by the flow model. Their positions are plotted every T' for a total time of $500T'$.

In simulating the motion of particles along streamlines we must also account for the changing height h of the free surface above the rotation center as a function of tumbler orientation. For example, Figs. 1(b) and 1(c) show a square tumbler in which h decreases significantly after 1/8th of a revolution. If h is decreasing and v_y is positive, particles near the free surface could leave the flowing layer. To prevent this the time derivative of the height $\dot{h}$ is added to v_y in Eq. (3).

The Poincaré section for a time independent velocity field, such as the half-full circular tumbler in Fig. 2(a), consists entirely of regular flow regions with closed loops corresponding to streamlines (here we arbitrarily choose $T'=T/2$ since N is infinite). For time periodic flow, see, for example, the square tumbler flow in Fig. 2(b), particle trajectories are time dependent and the streamlines associated with different times (or equivalently different tumbler orientations) cross.

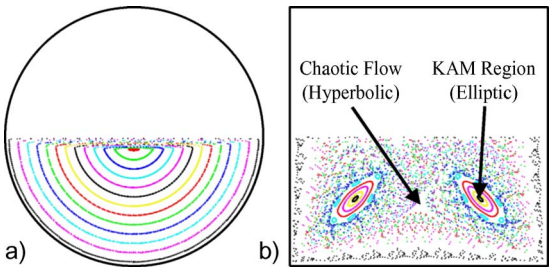

FIG. 2. (Color online) Computationally derived Poincaré sections for (a) a circular tumbler and (b) a square tumbler. Note in (b) the lobes of regular flow surrounded by a chaotic region.

One consequence of time-periodic velocity fields is the emergence of periodic points. A point is said to be periodic with period n if a particle initially at that point returns to it after nT'. These points are either elliptic or hyperbolic. For elliptic points, the nearby linearized flow is a rotation. Figure 2(b) shows that the elliptic point and a region of regular flow surrounding it, known as the Kolmogorov-Arnol'd-Moser (KAM) region, are separated from the rest of the flow by a boundary which no particles cross in the absence of diffusion. For hyperbolic points, the nearby linearized flow is stretched in one direction and compressed in another. These dynamics lead to stretching and folding and to chaotic mixing [16]. The hyperbolic point shown in Fig. 2(b) lies in a chaotic region.

B. Segregation model

The patterns generated by tumbling a mixture of two different particle types result from the interplay of advection, collisional diffusion, and segregation; the latter are assumed to act only in the flowing layer. To combine these elements in a single model we treat advection separately from segregation and diffusion. As was the case for the calculation of the Poincaré sections, we consider finite populations of particles advected by the continuum velocity field developed above for identical particles. Segregation is included by allowing the distinct populations to interact locally, while diffusion is added as a Langevin term to the advection equations.

We first address segregation where pure S systems and pure D systems provide two limiting examples of segregating mixtures. Segregation models for S systems are in general more complicated than those for D systems. For example, Khakhar *et al.* have proposed a model for S systems based on a statistical mechanics approach [17]. We will demonstrate by means of experiment and simulation that although the driving forces of segregation in S and D systems are undoubtedly different, the resulting (steady) segregation patterns are almost identical. Therefore we use a simple and well tested D system segregation model that employs an effective buoyancy mechanism based on the local number den-

sity of more dense particles f and a characteristic velocity

$$v_0 = \frac{2\beta(1-\bar{\rho})D_{\text{coll}}}{d},$$

where β is a constant of $O(1)$, $\bar{\rho}$ is the density ratio of light to heavy particles, and D_{coll} is the collisional diffusivity. Specifically, the vertical "drift velocities" are

$$\dot{y}_{dm} = -v_0(1-f), \tag{4a}$$

$$\dot{y}_{dl} = v_0 f \tag{4b}$$

for more and less dense particles, respectively. Savage [18] used hard-sphere particle dynamic models to obtain an expression for the diffusivity

$$D_{\text{coll}} = g(\eta)d^2\dot{\gamma}, \tag{5}$$

where the shear rate is $\dot{\gamma}=dv_x/dy$ and $g(\eta)$ is a function of the solids volume fraction η. Since D_{coll} is independent of particle density we assume it to have the same value for both particle types used in our model. [Note that we do not calculate D_{coll} using Eq. (5)—see below.] For our model $v_x \propto y$ which implies that $\dot{\gamma}$ is constant. Consequently, Eqs. (4) depend only on f. We discuss the calculation of f and our specific choice for the functional dependence of the drift velocities on f in greater detail below and in the Appendix.

Collisional diffusion is incorporated into the model by adding a small random velocity component S in the y direction to particles within the flowing layer. S is drawn from a Gaussian velocity distribution with variance $2D_{\text{coll}}/\Delta t$, where Δt is the simulation time step.

The velocities associated with segregation and diffusion are added to the y components of the velocity but not to the x components. This omission can be understood by examining the Péclet number (Pe) which characterizes the ratio of convective to diffusive transport. Here we use it to quantify the relative strengths of segregation and diffusion in comparison to advection. According to Eq. (4), $\dot{y}_{dm}$ and $\dot{y}_{dl}$ are directly proportional to D_{coll}. For the tumbler system, Pe $=uL/D_{\text{coll}}$. In the x direction, uL is large compared to D_{coll} so Pe $\gg 1$. For this reason, segregation and diffusion in the x direction can be ignored.

The complete D system advection, diffusion, and segregation model is then specified by the particle velocity at a point (x,y). In the fixed bed particles move in pure solid body rotation with radial velocity $\omega\sqrt{x^2+y^2}$. In the flowing layer, particle velocities in the y direction are given by

$$\dot{y}_m = -\omega x\left(\frac{y_m}{\delta}\right)^2 + S + \dot{h} - v_0(1-f), \tag{6a}$$

$$\dot{y}_l = -\omega x\left(\frac{y_l}{\delta}\right)^2 + S + \dot{h} + v_0 f \tag{6b}$$

for more and less dense particles, respectively.

C. Simulation details

For all simulations the system is rotated with a constant angular velocity of $\omega=2\pi$. In regular polygonal shapes the center-to-corner distance is 1 so that $L(t)\leqslant 1$. Particle trajectories in the flowing layer are calculated by integrating Eqs. (2) and (6) for segregation or Eqs. (2) and (3) with the addition of the $\dot{h}$ term (computed with a forward Euler method) for Poincaré sections. A fourth-order Runga-Kutta scheme is used with a time step of $\Delta t=10^{-6}$. In the fixed bed, positions are converted to polar coordinates and updated using a forward Euler method with the same time step. Since the fill fraction is constant, $h(t)$ and $L(t)$ are computed for each orientation using geometrical arguments.

For segregation simulations a mixture of 1/3 heavy and 2/3 light particles is used. The number of particles is determined by the fill fraction and the particle diameter $d=0.016$. Particles are initially placed on a close packed hexagonal lattice. The segregation model parameters are $\beta=2$, $\bar{\rho}=0.5$, and Pe$=100$. D_{coll} is determined from $D_{\text{coll}}=uL/\text{Pe}$ and has a value of $\pi/10$ for our choice of parameters. Simulations are typically run for ten rotations, while patterns become periodic after about five rotations.

The concentration of more dense particles f at each time step and for each particle is computed by finding all "relevant" neighboring particles whose centers are less than $1.5d$ away and then calculating the fraction of more dense particles. For less (more) dense particles the relevant neighbors lie above (below). The motivation for this particular protocol is discussed in the Appendix.

IV. RESULTS: FILL FRACTION OF ONE-HALF

In this section experiment and simulation are used to examine segregation in half-full ($\phi=0.5$) polygonal tumblers with even and odd numbers of sides (see Figs. 3 and 4, respectively). In columns from left to right the figures present images of the experiment, computationally generated Poincaré sections, and results from simulations of the continuum segregation model.

A. Even-sided tumblers

Consider first tumblers with an even number of sides as shown in Fig. 3. Experimental and computational results both exhibit segregation with the formation of a multilobed core of small or dense particles, respectively, which reaches steady state within a couple of revolutions. Each core has $N/2$ lobes that point toward a tumbler corner, and each lobe passes through the flowing layer twice per tumbler revolution. In the square and hexagonal tumblers, the lobes are curved such that they are asymmetrical about the diagonals. While the patterns change during rotation as lobes pass through the flowing layer, the patterns are the same at the end of each flow period T'.

The Poincaré sections reveal elliptic points surrounded by relatively large islands of regular flow (KAM regions) located halfway along the diagonals between the center and the corners of the tumbler. The elliptic points have period $T/2$ which we characterize as a multiple n of the temporal periodicity of the stream function T'. For these elliptic points $n=N/2$. Their associated islands are readily identified with the lobes in the segregation patterns. (Note that for the par-

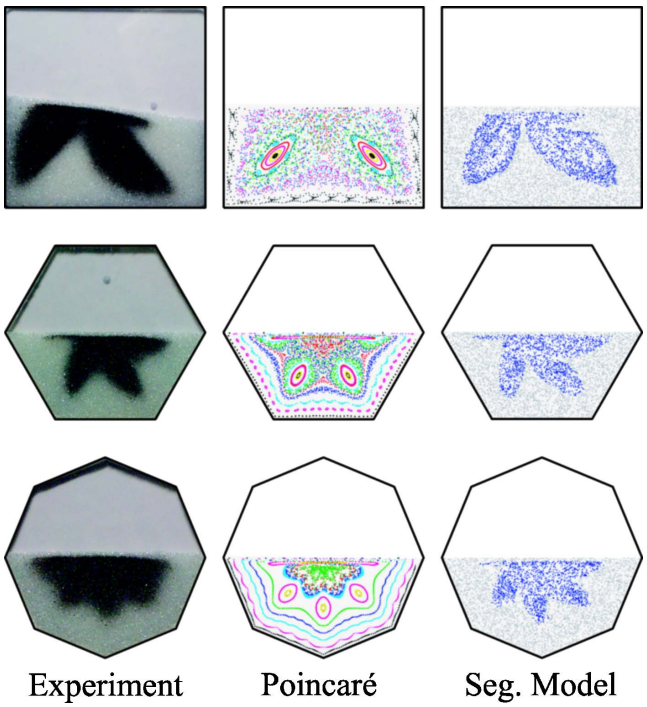

FIG. 3. (Color online) Half-full polygonal tumblers with an even number of sides. Left column: Experimental size segregation results. Center column: Poincaré sections from simulation. Right column: Density segregation results from simulation.

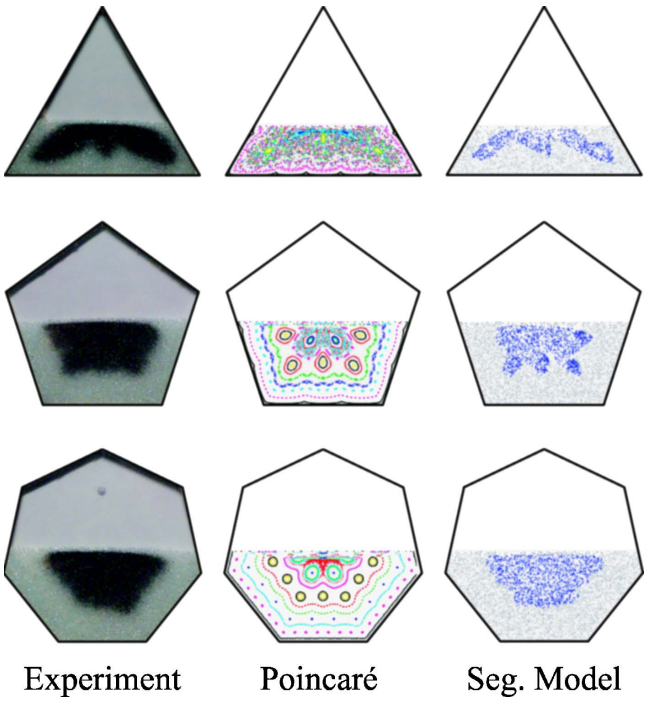

FIG. 4. (Color online) Half-full polygonal tumblers with an odd number of sides. Left column: Size segregation experiment results. Center column: Poincaré sections from simulation. Right column: Density segregation simulation results.

ticular configurations of the hexagonal and octagonal tumblers shown in Fig. 3 a lobe is passing through the flowing layer and the associated elliptic point is located at the center of the flowing layer. When the tumbler is rotated slightly further, the elliptic point returns to the diagonal.) Most areas around the KAM regions exhibit chaotic flow. Closer to the edges of the tumbler there are additional areas of regular flow with streamlines reminiscent of those found in the circular tumbler (see, for instance, the octagonal tumbler in Fig. 3). The regions near the edges of the hexagonal tumbler show higher period elliptic points surrounded by small KAM regions. However, in light of collisional diffusion and segregation, these small regions are not expected to play a major role in the segregation process unless the ratio of small (heavy) to large (light) particles is very large. Generally, the relative tumbler area that exhibits chaotic flow decreases as the number of sides is increased.

B. Odd-sided tumblers

Segregation patterns in odd-sided tumblers are shown in Fig. 4 and reveal different structure than in the even-sided tumblers. The segregation data from experiment and simulation again show a distinct core but with a shape resembling the container and with mostly smaller lobes (e.g., $N=5$ and $N=7$ from experiment). For the triangle and pentagon there are N lobes where, in addition to lobes pointing toward the corners, there also exist additional smaller lobes directed towards the middle of each side (this is seen most clearly in the segregation simulations).

Poincaré maps again provide insight into the segregation structure. Large regular islands lie along the diagonals and along lines between the tumbler center and the middle of the sides. There are N associated elliptic points each with period N. These islands alternate between the diagonal and the middle of the side configurations on each successive pass through the flowing layer. Consequently, and unlike the case for even-sided polygons, each KAM region passes through the flowing layer twice (corresponding to a complete tumbler rotation) before returning to its original position. Near the center of the odd-sided tumblers there are $(N-1)/2$ additional smaller regular islands each with $n=N$. Note that for $\phi=0.5$ the segregation patterns are less structured in the odd-sided tumblers than in even-sided tumblers even though the layer height is a function of time in the former and constant in the latter. Additionally, despite the existence of obvious KAM regions, no clear lobe structure is evident in the segregation results for the heptagonal container.

V. RESULTS: FILL FRACTION GREATER THAN ONE-HALF

Previous results for both quasi-2D and -3D tumblers show that segregation patterns can be highly sensitive to fill fraction [19]. One important robust difference between $\phi=0.5$ and larger fill fractions occurs when, for large enough ϕ, the bottom of the flowing layer remains always above the center of tumbler ($\delta_0<h$). In this case, particles surrounding the center never pass through the flowing layer which results in an unmixed core. The shapes of these cores usually resemble

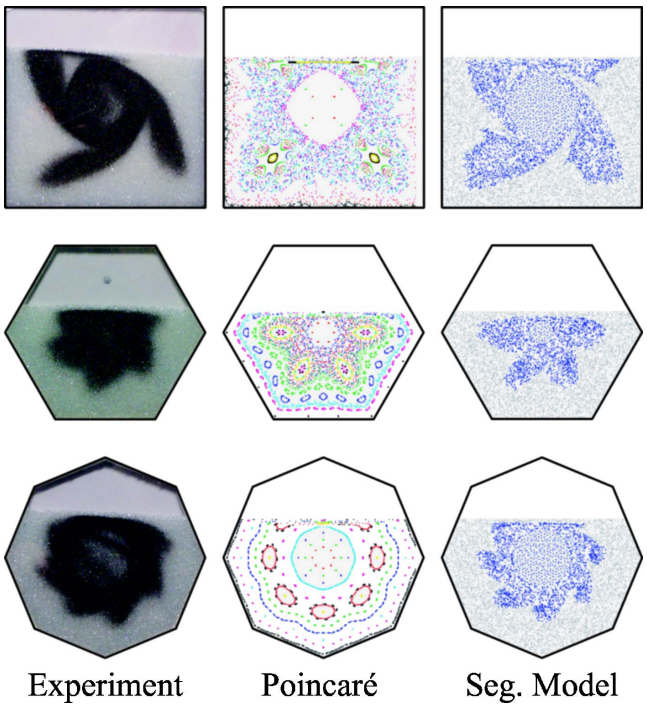

FIG. 5. (Color online) Even-sided polygonal tumblers with fill fractions of 75% (square), 65% (hexagon), and 75% (octagon). Left column: Size segregation experiment results. Center column: Poincaré sections from simulation. Right column: Density segregation simulation results.

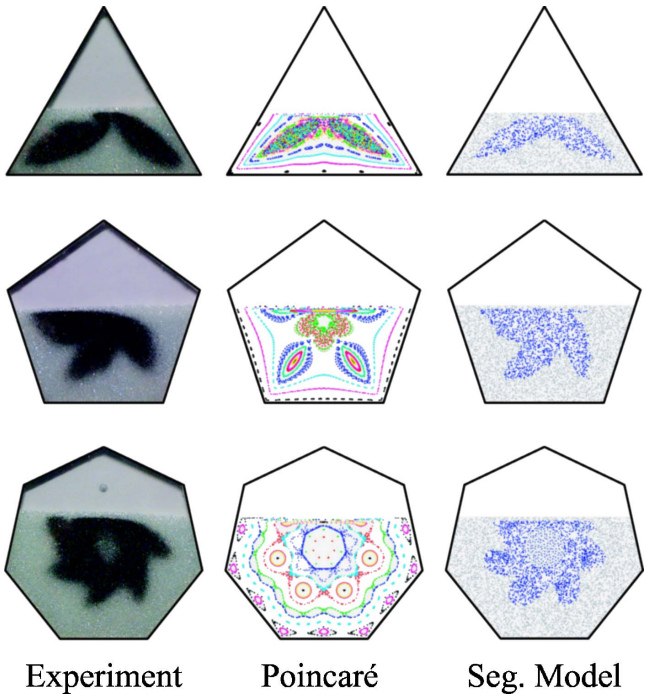

FIG. 6. (Color online) Odd-sided polygonal tumblers with fill fractions of 60% (triangle), 60% (pentagon), and 70% (heptagon). Left column: Size segregation experiment results. Center column: Poincaré sections from simulation. Right column: Density segregation simulation results.

that of the container but vary as ϕ is increased. In long duration experiments [$O(10^3)$ rotations] the core evolves due to creeping motion below the flowing layer [20], but these slow motions are not relevant in our relatively short duration simulations [$O(10)$ rotations].

A. Even-sided tumblers

The top row of Fig. 5 shows a square tumbler with $\phi=0.75$ in which three lobes form along the diagonals versus two lobes for $\phi=0.5$ (Fig. 3). The corresponding Poincaré section shows regular islands along the diagonals which have $n=3$. As with the half-full tumblers the lobes form near the islands and extend outward from a core of unmixed material. The curvature of the lobes is even more apparent here than with the half-full cases shown in Fig. 3. The hexagonal and octagonal tumblers also show an increase in the number of lobes with larger ϕ—Fig. 5 presents examples with four and six lobes, respectively. Again the lobes appear to match up with regular islands in the Poincaré sections and have n equal to the number of lobes. In all these examples a KAM region takes more than half of a tumbler rotation to return to its original position.

B. Odd-sided tumblers

As the fill fraction is increased for odd-sided tumblers the segregation patterns exhibit a variety of behaviors. Figure 6 presents a triangular tumbler with two lobes, a pentagonal tumbler with three lobes, and a heptagonal tumbler with five lobes. The lobes are much more pronounced than for the corresponding shapes with $\phi=0.5$. The corresponding Poincaré sections show regular islands occurring only along the diagonals. As with even-sided tumblers the segregation results for these cases exhibit lobe formation around the islands. For all cases n equals the number of lobes.

When lobes form only on the diagonals, the number of lobes that pass through the flowing layer per rotation equals N independent of the container shape. For example, the pentagonal tumbler with $\phi=0.6$ in Fig. 6 has three lobes that pass through the flowing layer five times per rotation so that each lobe passes through the layer an average of $5/3$ times per rotation. In general the elliptic points corresponding to N_L lobes lying only along the diagonals have period N_L, or equivalently take a time $(N_L/N)T$ to return to their initial positions, and pass through the flowing layer N/N_L times each tumbler revolution. The maximum number of lobes lying solely on the diagonals is $N-1$. Thus, as the number of lobes increases, particles make fewer passes per rotation through the flowing layer which slows segregation requiring more rotations to reach a steady state.

C. Segregation in the pentagonal tumbler

To better understand how segregation varies with fill fraction we examine the pentagonal tumbler for increasing ϕ. As shown earlier in Fig. 4, the half-full tumbler has elliptic points with $n=5$ and a core that is roughly pentagonal in shape with little apparent lobe structure in the segregation pattern. As the fill fraction is increased to $\phi=0.55$, Fig. 7

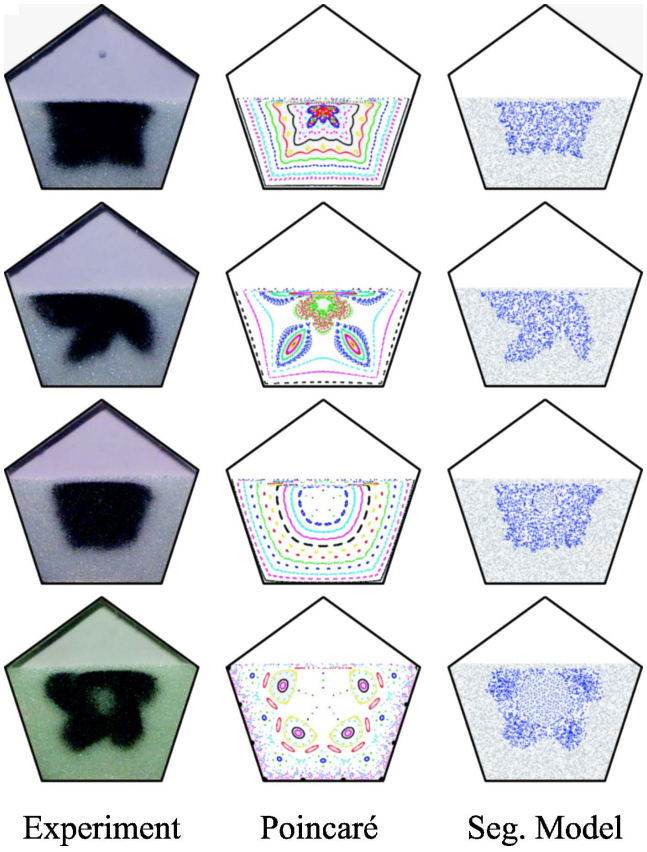

FIG. 7. (Color online) The evolution of segregation patterns in a pentagonal tumbler as fill fraction is increased. The fill fractions are 55, 60, 65, and 75 % from top to bottom. Left column: Size segregation experiment results. Center column: Poincaré sections from simulation. Right column: Density segregation simulation results.

indicates that the Poincaré map passes through a state with regular rings similar to those in a circular tumbler. Despite the dramatic differences between the Poincaré sections for $\phi=0.5$ and 0.55, the segregation patterns are nearly identical. As ϕ is increased to 0.6, 3 regular islands form along the diagonals of the Poincaré section, and the segregation pattern develops three large amplitude lobes. The corresponding KAM regions form at the edge of the unmixed core and move along the diagonals towards the corners with increasing fill fraction. At $\phi=0.65$ the three elliptic points and regular regions have moved to the corners and disappeared, and the system again enters a state of mostly radial segregation. With further increases in ϕ regular islands with $n=4$ develop just outside the unmixed core which results in the formation of four distinct lobes at $\phi=0.75$.

The same general process occurs for tumblers with different numbers of sides as the fill fraction is increased. Lobes wax then wane to a radial core matching the container shape. Further increases in ϕ produce lobes again but with N_L increased by one for patterns with lobes along the diagonals. The maximum number of diagonal lobes corresponds roughly to the number of tumbler corners that can be simultaneously covered by the grains. At some intermediate values elliptic points appear on the lines from the center to the middle of the sides. Sometimes lobes are associated with the corresponding KAM regions, but in other cases the core mimics the shape of the container.

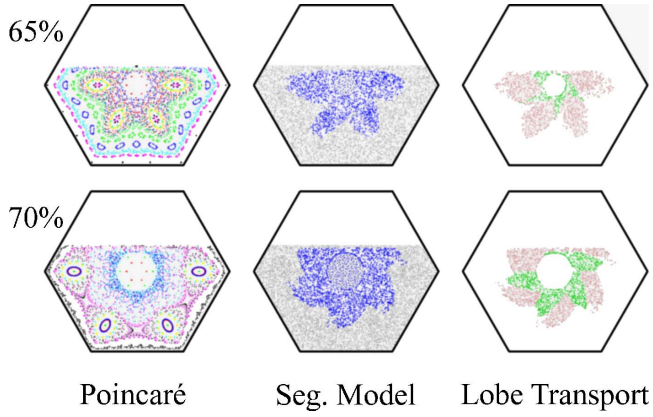

FIG. 8. (Color online) Interlobe transport in 65 and 70 % full hexagonal tumblers. Left: Poincaré sections from simulation. Center: Density segregation simulation result. Right: Lobe plot. Light colored particles remain in the same lobe in the next rotation while dark colored particles move to the next lobe.

D. Interlobe transport

The results presented above show a strong correlation between KAM regions in the Poincaré maps and segregation patterns even though the former are generated in the absence of the particle-particle interactions and particle diffusion included in the latter. As we now demonstrate, the presence and location of KAM regions relative to the lobes influences the flow in yet another way. Figure 8 shows steady state segregation patterns from simulations of two hexagonal tumblers with $\phi=0.65$ and $\phi=0.7$. Both tumblers generate four lobed segregation patterns with period four lobes, but there is an important difference between the two: for $\phi=0.65$ the lobes overlap the KAM regions while for $\phi=0.7$ they stretch toward but do not overlap these regions. To see the effect of this difference consider the motion of the heavy core particles that lie outside the unmixed core after one period of the elliptic points (2/3 of a rotation). The right column of Fig. 8 shows the final positions of the particles—particles that have moved from their original lobe are colored green (dark). For $\phi=0.65$ only a few particles near the core (19.4%) move to a new lobe, while for $\phi=0.7$ nearly twice as many particles (mainly along one side of each lobe) leave their initial lobe (36.3%). After eight four-period cycles, 43.5% of the particles in the 65% full tumbler leave their initial lobe while nearly all heavy particles (89.3%) switch to other lobes for the 70% full tumbler. Thus, despite the influence of diffusion and segregation, KAM regions located within lobes appear to limit the transport of particles between lobes.

VI. DISCUSSION: LOBE FORMATION

Our results demonstrate that segregation patterns in quasi-2D rotated tumblers are sensitive to container shape and fill fraction. Simulations of our segregation model accurately reproduce the steady state structures observed in ex-

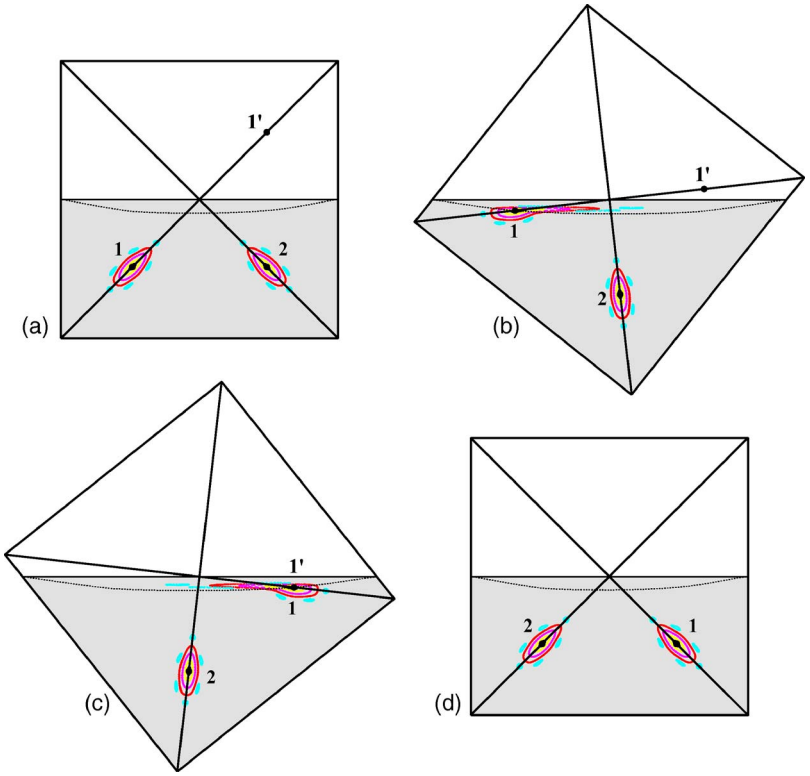

FIG. 9. (Color online) Mapping of elliptic points in a half-full square tumbler. (a) Initial condition with period-2 elliptic points along the diagonals. (b) Orientation at which point 1 enters the flowing layer. (c) Point 1 exits the flowing layer just as 1′, the new position of elliptic point 1 (advanced by 180°), rotates to the same position. (d) State after one period of flow. Points 1 and 2 have swapped positions.

periment. Further, the regular regions surrounding elliptic points in the Poincaré sections are clearly correlated with the lobe structure. Below we present a simple method of understanding the structure of the Poincaré maps and their sensitive dependence on the fill fraction. We then discuss various physical pictures of how the segregation mechanism contributes to the association of lobes with KAM islands. Finally we demonstrate how the relative proportion of small (more dense) to large (less dense) particles affects segregation patterns.

A. Periodic points

Poincaré maps exhibit structure throughout the entire occupied area of the tumbler. However, relative motion of particles, including mixing and segregation, occurs only when material is passing through the flowing layer. Therefore, insight concerning periodic (elliptic) points is gained by examining the changes in radial and relative angular positions that occur when particles transit the flowing layer. Consider first a half-full square tumbler which has period-2 elliptic points surrounded by KAM regions along the diagonals as illustrated in Fig. 9. A particle initially located on the left elliptic point at (1) [Fig. 9(a)] moves to the same location on the opposite (right) diagonal (1′) after each pass through the flowing layer (1/4 revolution) [Fig. 9(d)]. When the tumbler is rotated to the orientation where point 1 enters the flowing layer, as shown in Fig. 9(b), the particle begins moving relative to the container. Since the particle is at an elliptic point, the amount of time it takes a particle at point 1 to exit the flowing layer at the opposite end must equal the time for point 1′ to move to the bottom of the flowing layer via solid body rotation. Figure 9(c) shows the tumbler orientation where points 1 and 1′ have moved to the same location at the bottom of the flowing layer at the right side of the tumbler.

While the dynamics depicted in Fig. 9 require *a priori* knowledge of the elliptic point locations, the mapping technique can also identify elliptic points along the diagonal. Place a series of particles along the diagonal and rotate each one until it reaches the flowing layer. Calculate both the time it takes the particle to pass through the flowing layer using the velocity field in Eqs. (2) and (3) and the time for a point at the same relative position on the diagonal closest to the free surface to rotate to the bottom of the flowing layer. The solid curves in Fig. 10(a) show these two times as a function of the particle's initial radial distance along the diagonal r/L for $\phi=0.5$. The intersection of the two curves (labeled A) is the radial location of the elliptic point. Also, since the new diagonal is 180° from the initial one the elliptic point has period 2. For $\phi=0.55$ the flowing layer passage time is similar to the half-full case [dashed lines in Fig. 10(a)], but the time for the diagonal to rotate to the bottom of the flowing layer is reduced. This results in a periodic point (labeled B) that is closer to the center of the tumbler.

Figure 10(b) uses the method illustrated in Fig. 10(a) to locate all periodic points on diagonals as a function of fill fraction. The two cases from Fig. 10(a) are indicated with the labels A and B. Period-1 points are found near the corners for very low fill fractions, see, for example, Figs. 11(a) and 11(b). As ϕ is increased they move towards the center of the tumbler and disappear just before the system reaches half full. Period-2 points first appear in the corners of the tumbler $(r/L=1)$ at $\phi=0.4$. These points move rapidly inward as ϕ is increased, reaching the center at $\phi=0.59$. With further increases in ϕ, period-3 points form near the center of the tumbler and move outward as Figs. 11(c) and 11(d) show.

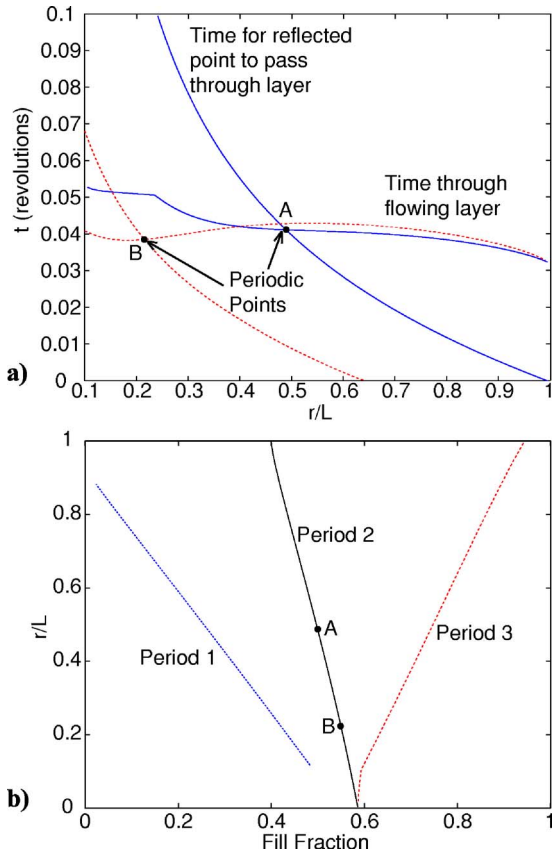

FIG. 10. (Color online) (a) Time for points to pass through the flowing layer and time for reflected points on diagonal to rotate to flowing layer bottom versus initial radial position along the diagonal for ϕ=0.5 (solid curves) and ϕ=0.55 (dashed curves) in a square tumbler. The intersection of the two curves locates the periodic points A and B for ϕ=0.5 and ϕ=0.55, respectively. (b) Periodic point location along diagonal vs ϕ. The left dashed, solid, and right dashed curves represent period-1, period-2, and period-3 points, respectively. Points A and B from (a) are shown on the period-2 curve.

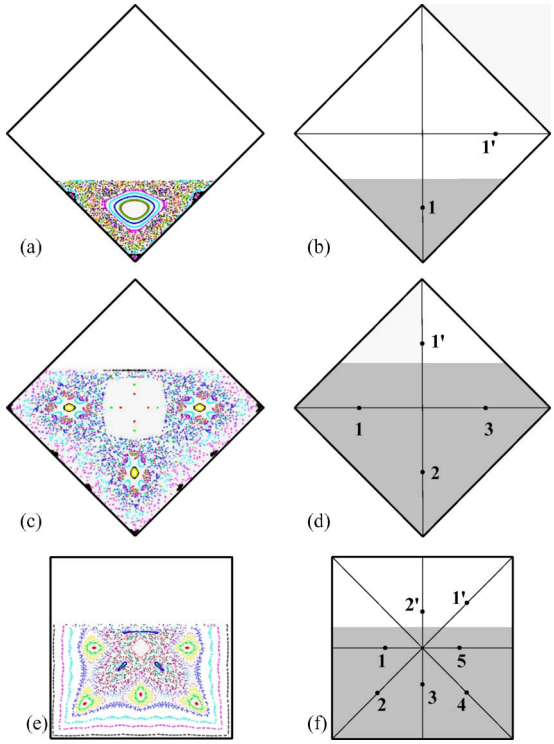

FIG. 11. (Color online) Relation between the number and periodicity of elliptic points and the fill fraction in a square tumbler. (a) Poincaré section for ϕ=0.2 and (b) corresponding period-1 elliptic point with future diagonal position (1′) which advances by 270°. (c) Poincaré section for ϕ=0.75 and (d) period-3 elliptic points with 1′ advanced by 90°. (e) Poincaré section with off-diagonal elliptic points for ϕ=0.63 and (f) period-5 points with 1′ advancing by 135°.

The period-3 points reach the edge at $\phi \approx 0.94$. Note that while period-3 points begin as soon as period-2 ones end, there is a region for $0.4 < \phi < 0.48$ in which period-1 and period-2 points coexist.

In addition to periodic points along the diagonals, higher order periodic points also exist. For ϕ=0.63 Figs. 11(e) and 11(f) show period-5 KAM regions with periodic points lying along both the diagonals and the normals to the side centers. At this value of ϕ, period-3 points simultaneously exist along the diagonals and are visible as the blue bounded regions near the center of Fig. 11(e). Other period-5 points such as those shown in Figs. 11(e) and 11(f) occur in a ϕ range that overlaps both the period-2 and period-3 regions. In Fig. 11(f), point 1 is initially located along a radius to the side center but moves to the diagonal 135° away. Conversely, point 2 is mapped from a diagonal to the side center normal. Since the center to edge distance differs between diagonals and normals we cannot immediately apply the same technique used above to locate the periodic points. However, the technique can be readily generalized to higher order periodic points by considering the motion after multiple passes through the flowing layer (2 in the present case).

This technique for understanding the location of periodic points is also readily applied to other regular polygons. Also notice that the flowing layer passage time curves [Fig. 10(a)] are essentially horizontal and only weakly dependent on the fill fraction and that subsequently most of the change in periodic point location is due to the shift in the curve associated with diagonal rotation. Consequently, the quantitative analysis of simple as well as higher order periodic points should be amenable to analytic techniques using iterated maps.

B. Volume fraction

We have presented numerous pieces of evidence indicating that segregation patterns are closely related to the structure of Poincaré sections. However, there are details for some shapes and fill fractions that are not observed in accord. For instance, the Poincaré map for the half-full pentagonal tumbler in Fig. 4 shows period-2 and period-5 KAM regions, but the segregation pattern exhibits just five small lobes. Similar situations may occur with even-sided tumblers such as the square with ϕ=0.63 that shows period-3 and -5 KAM regions. As another example, the ϕ=0.7 hexagon in Fig. 8 generates small lobes that do not reach the diagonals where

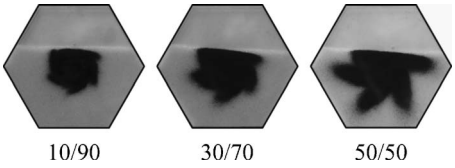

FIG. 12. Segregation patterns for a 70% full hexagonal tumbler with various mixtures of small and large particles. The percentage of small particles (by volume) are 10, 30, and 50 % from left to right.

the KAM regions are observed in the Poincaré section.

Throughout this paper, the relative composition of the granular material has been held constant at 1/3 small (heavy) particles and 2/3 large (light) particles. Figure 12 shows images from experiments in a hexagonal tumbler with $\phi=0.7$ for three *different* particle mixtures. The first image, with 10% small particles and 90% large particles by volume, displays only radial segregation. The second image, with 30% small particles, generates small lobes that point toward the edges. In the third image, a mixture with 50% small particles produces well defined lobes that stretch toward the corners of the tumbler and which are reminiscent of the patterns shown in Figs. 5 and 6.

We speculate that the observed lobe structure is also related to the relative size of the segregated core at fixed fill fraction. If the core is too small to reach the KAM regions the core will not exhibit lobes. Adding small particles increases the core size allowing it to reach out to the KAM region and form lobes. If the core completely engulfs the KAM regions lobes will not be visible. For fill fractions where multiple sets of elliptic points are present, the observed lobe structure will correspond to the elliptic points whose KAM regions are closest to the core boundary. Additionally, the images in Fig. 12 clearly show that the lobes do not extend directly along the diagonal but rather follow a curved path, similar to the asymmetry observed in the half-full square and hexagonal tumblers in Fig. 3. Insights can be made into the nature of the curvature by examining the regions of chaotic flow and the hyperbolic points that characterize them. This sensitivity to chaotic flow and small particle volume fraction is part of an ongoing study [21].

C. Segregation mechanisms

We have shown that segregation patterns are clearly correlated with the location of KAM regions, but we have not identified or described a physical mechanism that explains why this is the case. Various possibilities exist to explain the structure of segregation patterns. First, consider the tendency for the lobe patterns to extend from the center of the tumbler towards the corners. As the tumbler rotates toward a configuration where the free surface intersects the corner, the flowing layer grows in length and depth. As this occurs, the small (heavy) particles in the lower half of the flowing layer flow for more time and thus move closer to the edges. Conversely, as the free surface rotates out of the corner and the flowing layer shrinks, these particles leave the layer earlier and are closer to the center of the tumbler. The net result is lobe formation. However, this description does not explain the large variations in lobe size with ϕ—see, for example, Fig. 7.

Another mechanism is presented by Fiedor and Ottino for circular tumblers in which a modulated angular velocity generates lobes [14]. They argue that when the tumbler, and therefore the particles in the flowing layer, accelerates (equivalent to lengthening of the free surface in a polygonal tumbler as it approaches a corner) the segregation mechanism slows. For size segregation, this means that small particles travel farther before percolating to the bottom of the layer resulting in lobe formation in these areas. This explanation shows how a well mixed system could form lobes. However, the patterns shown in Figs. 3 and 7 develop independent of the initial conditions. For instance, if a well mixed system forms lobes, lobes will still form even if the initial condition is instead a segregated radial core.

Finally, rotated bidisperse systems are subject to mechanisms that mix as well as segregate. Consider the half-full square tumbler of Fig. 3 in which a large portion of the flow is chaotic, including the interface between segregated particles. Particles at the interface are driven to mix as well as segregate. The particle distributions evolve until an equilibrium is reached where as soon as particles at the interface mix, they unmix, leaving the interface stable. This results in an effective perimeter between the two phases even in the absence of a KAM boundary.

VII. CONCLUSIONS

Segregation of bidisperse particle mixtures in rotating, quasi-2D, regular polygonal tumblers is sensitive to tumbler shape, fill fraction, and particle concentration. The number, amplitude, and location of the lobes in the segregated core vary nonmonotonically with the fill fraction and with the tumbler shape for fixed fill fraction. Patterns in tumblers of different shape exhibit qualitatively similar behavior. Nearly all characteristics of the patterns are captured by a segregation model that combines advection by a continuum velocity field, random diffusion, and a particle interaction that drives segregation via an effective buoyancy mechanism.

Our research also reveals a strong connection between patterns observed in Poincaré sections generated by a continuum model and size segregation patterns observed in experiment as well as density segregation patterns found using the segregation model. Lobes of small (or more dense) particles occur around KAM regions observed in Poincaré sections. The location and number of elliptical points and associated KAM regions evolves with fill fraction, sometimes undergoing drastic changes for a very small change in fill fraction. If the KAM regions lie well within or far outside the segregated core mostly radial segregation with little or no lobe formation is observed. The location and period of elliptic points as a function of fill fraction and tumbler shape is captured by a simple model that compares the flowing layer passage times with the rotation of symmetry lines of the container. The results for the size segregation experiments and density segregation simulations match each other, suggesting that the segregation mechanism operates indepen-

dently of the driving forces. In fact, varying the density ratio from 0.1 to 0.95 in simulations had no impact on the final patterns. Possibilities for future work on segregation in quasi-2D polygonal tumblers include studies examining the role of the concentrations of large and small particles (in progress), iterated map models to fully capture the structure of the flow dynamics, and investigations of the effects of varying the size or density ratios on segregation structure and temporal evolution.

ACKNOWLEDGMENTS

We thank Devang Khakhar for useful discussions, Stan Fiedor for assistance with the experiments, and Steve Meier for sharing his data and assisting in the production of Fig. 12. This work was supported by the DOE through the Office of Basic Energy Sciences.

APPENDIX: SEGREGATION FLUX

The form of the segregation flux (drift velocities) in Eq. (6) is in some sense arbitrary. Here we first show that the final segregation patterns depend only weakly on the specific functional relation between the drift velocities and the local particle concentration. In our simulations the particle drift velocities in Eq. (4) are chosen proportional to $(1-f)^p$ and f^p with $p=1$ because these forms meet the conditions that $\dot{y}_{dm}$ and $\dot{y}_{dl}$ approach 0 for areas with pure species. However, any positive value of p will also satisfy these conditions.

For $p=0.25$, 0.5, 0.75, 1, 1.5, and 2 we have simulated segregation in a half-full square container and found the same two-lobed segregation pattern as shown in the first row of Fig. 3. The only significant difference between the various values of p is the time to reach this steady state, which we quantify using the degree of mixing M. For a given particle consider the number of neighboring particles (within a radius d) of the same type divided by the total number of neighboring particles—this quantity averaged over all particles is M. Figure 13 shows M versus time for various p. For all values of p we tested, M initially decreases linearly with a slope inversely proportional to p, and during this time the segregation is primarily radial. Slow oscillations of $O(1)$ in $M(t)$ indicate the formation of lobes. For $p \leqslant 1$ the oscillations

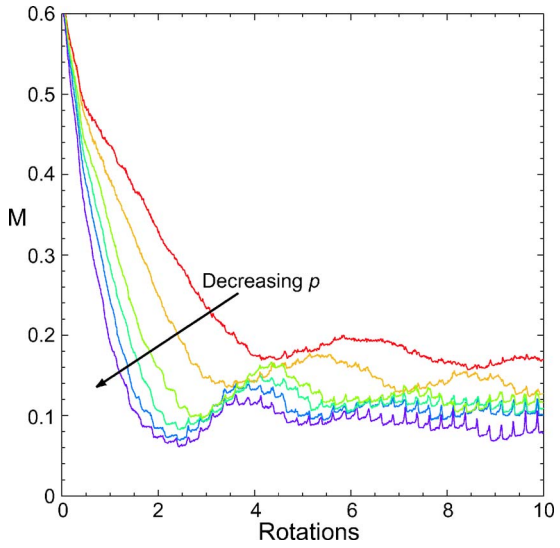

FIG. 13. (Color online) Degree of mixing versus time in a half-full square tumbler for different values of $p=\frac{1}{4},\frac{1}{2},\frac{3}{4}$, 1, $\frac{3}{2}$, and 2. For the simulation data shown the segregation drift velocities for heavy and light particles are proportional to $(1-f)^p$ and f^p, respectively.

decay and a similar final value of M is achieved after ten revolutions. For $p=3/2$ and 2 the oscillations in M are longer and decay more slowly; eventually they decay and M approaches the same value as for $p \leqslant 1$.

The choice of particle neighborhood has an influence on some details of the segregation patterns. Consider a configuration which should be stable: a sheared horizontal layer of segregated particles with light particles on the top and heavy particles on the bottom. With a circular neighborhood the segregation drift velocities are non-zero for particles at the interface and the layers repel. The resultant gap increases as the particles enter the fixed bed. A smaller radius neighborhood minimizes, but does not eliminate, the gap. However, by considering for light (heavy) particles only neighboring particles whose y positions are larger (smaller) the gap is removed. This semi-circular neighborhood is used in our segregation simulations. The resulting segregation patterns are virtually the same as those calculated with a circular neighborhood but without a gap between segregated regions.

[1] H. M. Jaeger, S. R. Nagel, and R. P. Behringer, Rev. Mod. Phys. **68**, 1259 (1996).
[2] H. Henein, J. K. Brimacombe, and A. P. Watkinson, Metall. Trans. B **14B**, 191 (1983).
[3] G. H. Ristow, *Pattern Formation in Granular Materials* (Springer, Berlin, 2000).
[4] J. Rajchenbach, Phys. Rev. Lett. **65**, 2221 (1990).
[5] D. V. Khakhar, J. J. McCarthy, T. Shinbrot, and J. M. Ottino, Phys. Fluids **9**, 31 (1997).
[6] D. V. Khakhar, J. J. McCarthy, and J. M. Ottino, Phys. Fluids **9**, 3600 (1997).
[7] K. M. Hill, D. V. Khakhar, J. F. Gilchrist, J. J. McCarthy, and J. M. Ottino, Proc. Natl. Acad. Sci. U.S.A. **96**, 11701 (1999).
[8] K. M. Hill, J. F. Gilchrist, J. M. Ottino, D. V. Khakhar, and J. J. McCarthy, Int. J. Bifurcation Chaos Appl. Sci. Eng. **9**, 1467 (1999).
[9] N. Jain, J. M. Ottino, and R. M. Lueptow, Phys. Fluids **14**, 572 (2002).
[10] T. S. Komatsu, S. Inagaki, N. Nakagawa, and S. Nasuno, Phys. Rev. Lett. **86**, 1757 (2001).
[11] H. A. Makse, Phys. Rev. Lett. **83**, 3186 (1999).
[12] D. V. Khakhar, A. V. Orpe, and J. M. Ottino, Adv. Complex

Syst. **4**, 407 (2001).
[13] T. Elperin and A. Vikhansky, Europhys. Lett. **42**, 619 (1998).
[14] S. J. Fiedor and J. M. Ottino, J. Fluid Mech. **533**, 223 (2005).
[15] N. A. Pohlman, S. W. Meier, J. M. Ottino, and R. M. Lueptow, J. Fluid Mech. **560**, 355 (2006).
[16] J. M. Ottino, *The Kinematics of Mixing: Stretching, Chaos, and Transport* (Cambridge Press, Cambridge, 1989).
[17] D. V. Khakhar, J. J. McCarthy, and J. M. Ottino, Chaos **9**, 594 (1999).
[18] S. B. Savage, *Disorder and Granular Media: Disorder, Diffusion and Structure Formation in Granular Flow* (Elsevier Science Publishers, Amsterdam, 1993), p. 255.
[19] J. F. Gilchrist and J. M. Ottino, Phys. Rev. E **68**, 061303 (2004).
[20] B. A. Socie, P. Umbanhowar, R. M. Lueptow, N. Jain, and J. M. Ottino, Phys. Rev. E **71**, 031304 (2005).
[21] S. W. Meier, S. E. Cisar, R. M. Lueptow, and J. M. Ottino, Phys. Rev. E **74**, 031310 (2006).